Journal of Magnetism and Magnetic Materials 532 (2021) 167936

Contents lists available at ScienceDirect

Journal of Magnetism and Magnetic Materials

journal homepage: www.elsevier.com/locate/jmmm

The magnetic phase diagram of $Sr_2Fe_3Ch_2O_3$ (Ch = S, Se)

H. Guo [a,b], M.T. Fernández-Díaz [c], K.T. Lai [a,1], M. Valldor [a,2], A.C. Komarek [a,*]

[a] Max-Planck-Institute for Chemical Physics of Solids, Nöthnitzer Str. 40, D-01187 Dresden, Germany
[b] Neutron Science Platform, Songshan Lake Materials Laboratory, Dongguan, Guangdong 523808, China
[c] Institut Laue-Langevin (ILL), 71 avenue des Martyrs, F-38042 Grenoble Cedex 9, France

ARTICLE INFO

Keywords:
Magnetism
Iron chalcogenide
Spin structure
Neutron diffraction
Phase diagram

ABSTRACT

We here report on the complex magnetic structures within the $Sr_2Fe_3Ch_2O_3$ (Ch = S and Se) system that we studied by means of powder neutron diffraction. Successive magnetic transitions occur in the magnetic phase diagram of both compounds with an incommensurate character of the magnetic structure at higher temperatures and a lock-in to commensurate low temperature structures. The commensurate propagation vector for the Ch = S compound is different from the Se containing compound which could be indicative for changes in the size of competing exchange interactions implied by structural changes within the two materials.

1. Introduction

At the crossover between one-dimensional (1D) chains and two-dimensional (2D) lattices, ladders have attracted considerable attention in the past [1]. For S = 1/2 ladder systems the ground states depend on the even or odd number of legs that occur - with the former one exhibiting short range spin correlations only and with the latter one resembling 1D chain systems [1]. Depending on the presence of an inter-ladder coupling, also long range magnetic order can be observed at low temperatures. Very recently, the Fe^{2+} spin ladder compound $BaFe_2S_3$ has attracted attention due to the observation of superconductivity at elevated pressures [2]. $Sr_2Fe_3S_2O_3$ and $Sr_2Fe_3Se_2O_3$ are also Fe^{2+} compounds that have been discovered recently [3]. Probably with regard to the bare Fe-O skeleton these materials have been called spin ladder compounds [3]. We will here also refer to this labeling. The magnetic structure of one of these two compounds - $Sr_2Fe_3Se_2O_3$ - was already studied in detail [4] and is quite complex and changes its nature from incommensurate to commensurate with temperature [4]. Here, we report on the magnetic structure of the isostructural sulfide compound, $Sr_2Fe_3S_2O_3$, and compare the magnetic phase diagrams of both materials. Both compounds crystallize in the orthorhombic structure (*Pbam*) with two distinct Fe sites - Fe1 at the 2a and Fe2 at the 4h site, see Fig. 1. The Fe2 ions are meri-octahedrally coordinated by O and *Ch* ($Fe2Ch_3O_3$). The Fe2 ions are associated with the 2-leg ladder frame running along the *c*-direction. The Fe1 ions are octahedrally coordinated and form $Fe1Ch_4O_2$ compressed trans-octahedra that are face-sharing with the $Fe2Ch_3O_3$ octahedra. Note, that changes of the magnetism induced by Se-S substitution (accompanied by an expansion of the crystal lattice) are not uncommon [5].

2. Experimental

Polycrystalline samples of $Sr_2Fe_3Se_2O_3$ and $Sr_2Fe_3S_2O_3$ were synthesized as described elsewhere. [3] Powder neutron diffraction measurements were performed on the D1B diffractometer at the Institut Laue-Langevin (ILL) in Grenoble, France. Powder samples were loaded into a vanadium can. A neutron wavelength of 2.52 Å was selected by the pyrolytic graphite (002) monochromator. The patterns were collected either during warming up with a small ramping rate (0.4–1 K/min), or at characteristic temperatures with long counting times. Magnetic structure refinements were performed using the *Fullprof* suite [6], together with *Sarah* [7] for symmetry analysis.

3. Results and discussion

The temperature dependence of the neutron diffraction patterns are shown in Fig. 2. With a decrease in temperature, additional magnetic reflections appear below $T_{inc} \sim 120$ K for both compounds. At lower

* Corresponding author.
E-mail address: Alexander.Komarek@cpfs.mpg.de (A.C. Komarek).
[1] Present address: Department of Physics, The Chinese University of Hong Kong, Shatin, Hong Kong.
[2] Present address: Centre for Materials Science and Nanotechnology (SMN), Department of Chemistry, University of Oslo, P.O. Box 1033 Blindern, N-0315 Oslo, Norway.

https://doi.org/10.1016/j.jmmm.2021.167936
Received 5 October 2020; Received in revised form 4 January 2021; Accepted 13 March 2021
Available online 2 April 2021

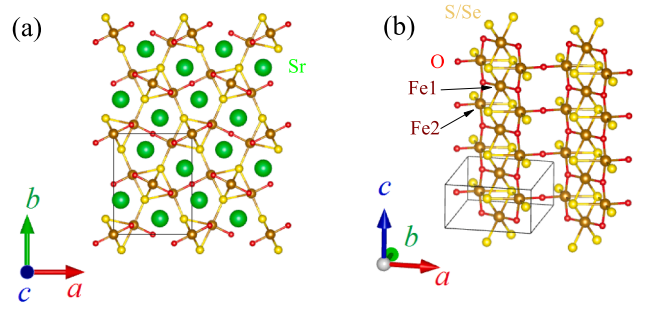

Fig. 1. Crystal structure of $Sr_2Fe_3Ch_2O_3$. (a) A view along the *c* direction. (b) A 3D view showing the typical ladder structure running along the *c* axis. For simplicity, the Sr ions are ignored.

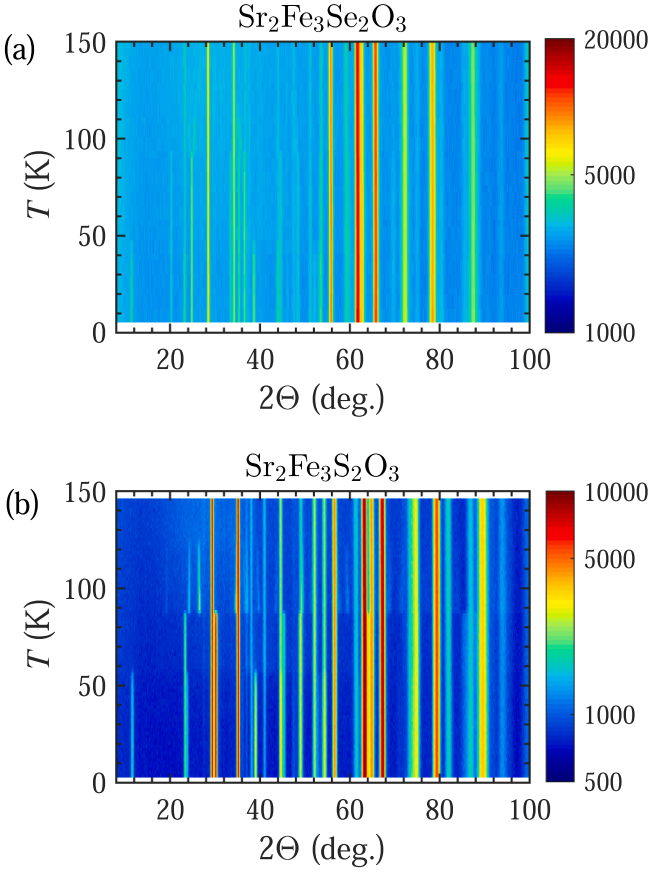

Fig. 2. Temperature dependence of the NPD patterns for (a) $Sr_2Fe_3Se_2O_3$ and (b) $Sr_2Fe_3S_2O_3$.

temperatures, a lock-in transition occurs with the appearance of a different set of magnetic reflections below T_1. For even lower temperatures, below T_2, extra magnetic reflections can be observed and coexist with the ones already occuring below T_1. The temperature dependence of the integrated peak intensities is shown in Fig. 3. A fit to $I = I_0(1 - T/T_0)^{\beta}$ yields the transition temperatures as summarized in Table 1 for both compounds. The values for the Se compound are roughly consistent with the one reported in Ref. [4]. The small discrepancies, especially for T_2, might be attributed to the fact that our patterns were measured during the warming process (with 6 K steps).

The diffraction data of both compounds measured above T_{inc} is in agreement with the reported orthorhombic structure with space group *Pbam* [3,4]. Some minor impurity phases can be identified such as SrSe

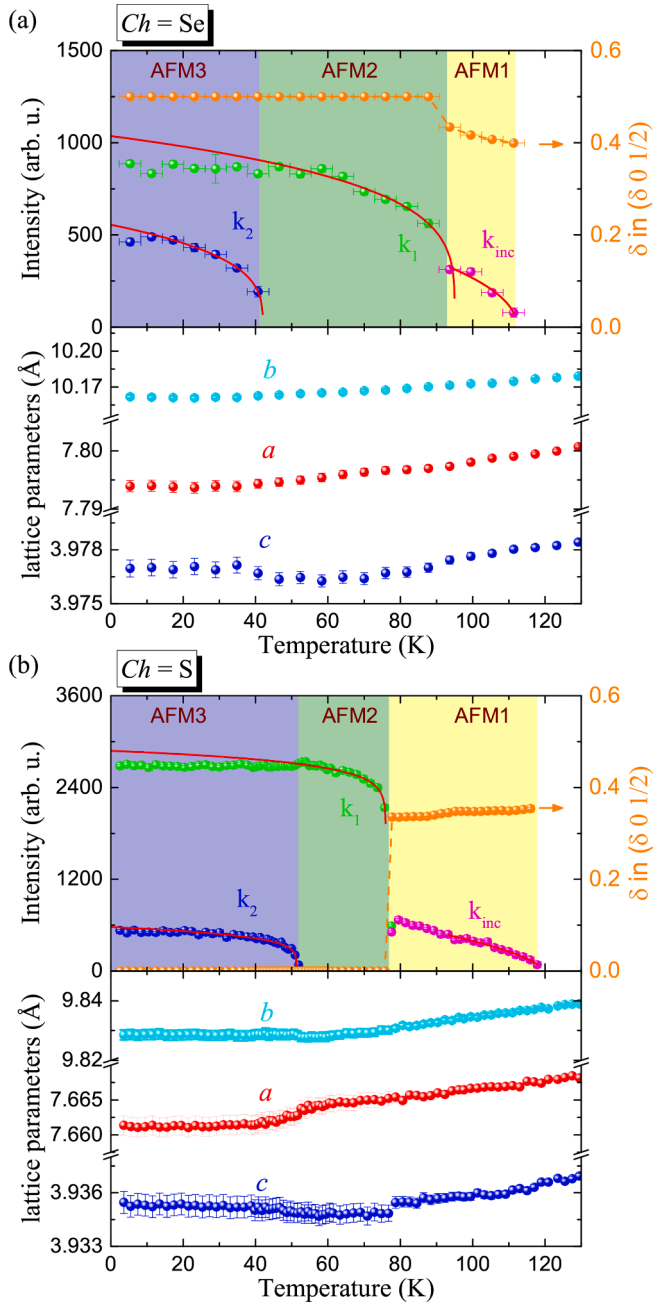

Fig. 3. Temperature dependence of the integrated peak intensities. The intensities for k_{inc}, k_1 and k_2 were taken from the peaks (a) centered at $2\Theta \sim 26°$, 25° and 11.5° for *Ch* = Se and (b) centered at $2\Theta \sim 26.5°$, 30.5° and 12° for *Ch* = S. The red curves are guide to the eyes. Additionally, the incommensurabilities δ are shown. Finally, the temperature dependence of the lattice constants is shown for each sample.

Table 1
Summary of the transition temperatures for both compounds. The numbers in the brackets indicate the standard error of the fit.

	T_{inc} (K)	T_1 (K)	T_2 (K)
Ch = Se	112(3)	95(7)	42.0(4)
Ch = S	119(1)	76.0(2)	52.51(6)

(0.76(9) wt%) and $SrFe_2Se_2O$ (0.98(19) wt%) for the Se compound, and $SrFe_2S_2O$ (0.95(10) wt%) and FeO (0.30(3) wt%) for the S compound, see Figs. 4(a) and 5(a). The magnetic structure of $SrFe_2Se_2O$ and

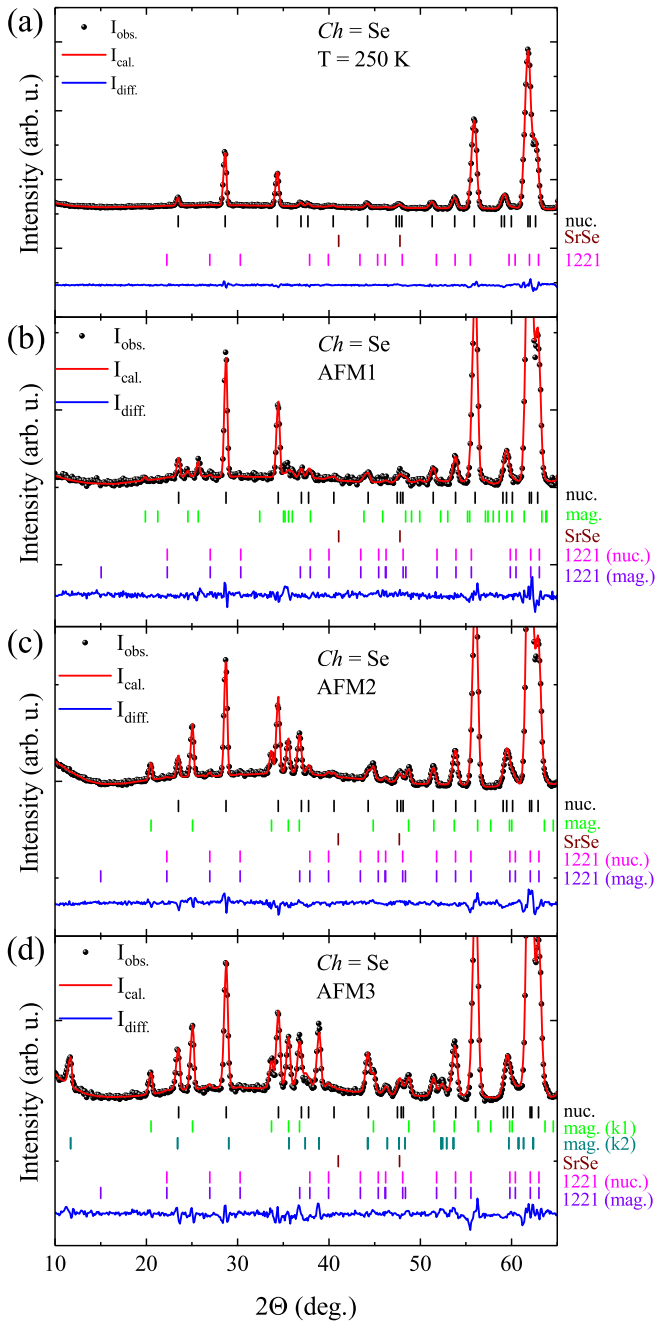

Fig. 4. Rietveld refinement patterns for the $Ch = Se$ sample. (a) At 250 K in the paramagnetic regime; (b) At 105 K between T_{inc} and T_1 with $R_{mag} = 37.7\%$; (c) At 79 K between T_1 and T_2 with $R_{mag} = 13.3\%$; (d) At 2 K below T_2 with $R_{mag1} = 10.4\%$ and $R_{mag2} = 12.9\%$.

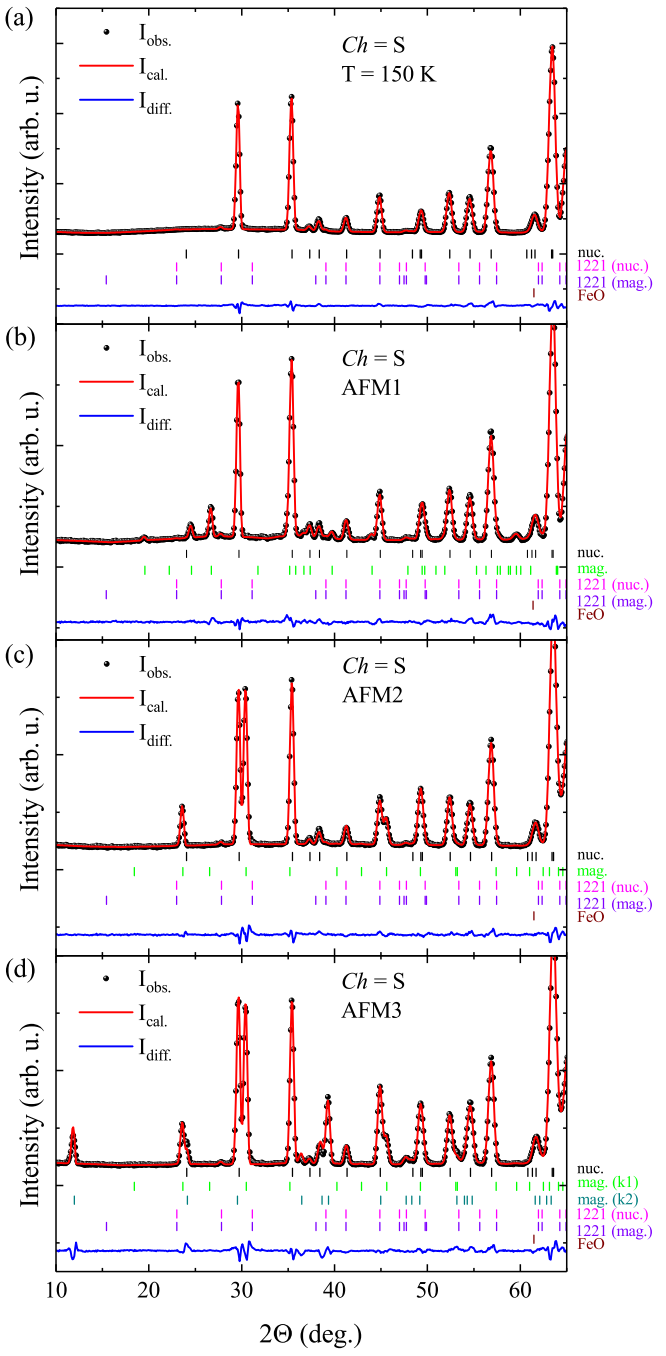

Fig. 5. Rietveld refinement patterns for the $Ch = S$ sample. (a) At 150 K in the paramagnetic regime; (b) At 96 K between T_{inc} and T_1 with $R_{mag} = 21.2\%$; (c) At 63 K between T_1 and T_2 with $R_{mag} = 3.1\%$; (d) At 2 K below T_2 with $R_{mag1} = 3.39\%$ and $R_{mag2} = 9.46\%$.

$SrFe_2S_2O$ has been reported [8] and taken into account within refinements as well.

3.1. A. $T_1 < T < T_{inc}$

The magnetic reflections in this temperature regime for both compounds can be characterized by an incommensurate propagation vector $\mathbf{k_{inc}} = (\delta, 0, 1/2)$. The incommensurability δ amounts to ~ 0.42 for the Se compound at 105 K and ~ 0.35 for the S compound at 96 K. The incommensurability δ for the Se compound evolves smoothly from ~ 0.39 at 111 K to the commensurate value 0.5 below T_1. On the other hand, the propagation vector is quite robust for the S compound, with $\mathbf{k}_{\text{inc}} \sim (0.35, 0, 1/2)$ in the $T_1 < T < T_{inc}$ regime. Below T_1 it undergoes an abrupt, first-order-like transition to the commensurate propagation vector (0, 0, 1/2).

Magnetic structure refinements were performed based on irreducible representation analysis. For the Fe1 and Fe2 ions at the *2a* and *4h* sites the magnetic representations decompose into four IRs as:

$$\Gamma_{\mathbf{k}_{inc}}(\text{Fe1}) = \Gamma_1^1 + 2\Gamma_2^1 + \Gamma_3^1 + 2\Gamma_4^1 \quad (1)$$

$$\Gamma_{\mathbf{k}_{inc}}(\text{Fe2}) = 2\Gamma_1^1 + \Gamma_2^1 + 2\Gamma_3^1 + \Gamma_4^1 \quad (2)$$

The superscript indicates the dimension of the IR. Note, that the Fe2 site splits into two orbits, which form the same IRs. The basis vectors (BV) for each IR are listed in Table 2. As reported in Ref. [4] only the Fe2

Table 2
Nonzero IRs together with basis vectors φ_ν for the Fe2 ions at the *4h* site in $Sr_2Fe_3Ch_2O_3$ with space group *Pbam* and propagation vector $\mathbf{k}_{inc} = (\varepsilon, 0, 1/2)$. The *4h* site splits into two orbits, e.g., with (x, y, z) = (0.2633, 0.0940, 0.5000) and (−0.2633, −0.0940, 0.5000) for *Ch* = Se. The parameters α and β are nonzero and constrained by $\alpha^2 + \beta^2 = 1$.

IRs	φ_ν	component	(x, y, z)	(x + 1/2,-y + 1/2,-z)
Γ_1	φ_1	Real	(1 0 0)	(α 0 0)
		Imag	(0 0 0)	(-β 0 0)
	φ_2	Real	(0 1 0)	(0 -α 0)
		Imag	(0 0 0)	(0 β 0)
Γ_2	φ_3	Real	(0 0 1)	(0 0 -α)
		Imag	(0 0 0)	(0 0 β)
Γ_3	φ_4	Real	(1 0 0)	(-α 0 0)
		Imag	(0 0 0)	(β 0 0)
	φ_5	Real	(0 1 0)	(0 α 0)
		Imag	(0 0 0)	(0 -β 0)
Γ_4	φ_6	Real	(0 0 1)	(0 0 α)
		Imag	(0 0 0)	(0 0 -β)

sites order above T_2. Following the analysis in Ref. [4] our refinements for both compounds show that the magnetic structure can be, indeed, described by the IR Γ_2 of Fe2. The moments are pointing along the *c*-axis with the magnitude sinusoidally modulated along the *a*-axis. The amplitudes are 2.12(7) μ_B for the *Ch* = Se compound at 105 K and 2.89(4) μ_B for the *Ch* = S compound at 79 K. The phase between the two orbits is negligibly small - thus, it was fixed to zero for the final refinement. The refined patterns are shown in Figs. 4(b) and 5(b), and the magnetic structure is shown in Fig. 6(a).

3.2. B. $T_2 < T < T_1$

With decreasing temperature below T_1 the propagation vector evolves from incommensurate to commensurate values. However, the commensurate propagation vectors for the two compounds turn out to be different - $\mathbf{k}_1 = (1/2, 0, 1/2)$ for the *Ch* = Se and $\mathbf{k}_1 = (0, 0, 1/2)$ for the *Ch* = S compound. The symmetry analysis for the Fe2 sites yields:

$$\Gamma_{\mathbf{k}_1}(\text{Fe2}) = 4\Gamma_1^2 + 2\Gamma_2^2 \tag{3}$$

for the *Ch* = Se compound, and

$$\Gamma_{\mathbf{k}_1}(\text{Fe2}) = 2\Gamma_1^1 + \Gamma_2^1 + 2\Gamma_3^1 + \Gamma_4^1 + \Gamma_5^1 + 2\Gamma_6^1 + \Gamma_7^1 + 2\Gamma_8^1 \tag{4}$$

for the *Ch* = S compound. The BVs for each IR are listed in Table 3 and Table 4. The magnetic moments are constrained within the *ab*-plane and along the *c*-axis for Γ_1 and Γ_2, respectively, for the Se compound. Following the lock-in transition from the higher temperature phase, the moments are also pointing along the *c*-axis in this regime (described by Γ_2) see Fig. 4(c). The magnetic moment amounts to 2.78(3) μ_B/Fe2 at 79 K and the corresponding magnetic structure is shown in Fig. 6(b).

The best refinement for the *Ch* = S compound could be achieved with the IR Γ_7 associated with the Fe2 ions only, see Fig. 5(c). The corresponding magnetic structure is shown in Fig. 6(c). The refined magnetic moment amounts to 3.21(1) μ_B/Fe2 at 63 K.

3.3. C. $T < T_2$

Below T_2, extra magnetic reflections appear and coexist with the ones characterized by $\mathbf{k}_1$. These additional reflections can be indexed by another propagation vector $\mathbf{k}_2 = (1/2, 1/2, 0)$ for both compounds. Symmetry analyses for both the Fe1 and Fe2 sites yield:

$$\Gamma_{\mathbf{k}_2}(\text{Fe1}) = \Gamma_1^1 + 2\Gamma_3^1 + 2\Gamma_5^1 + \Gamma_7^1 \tag{5}$$

$$\Gamma_{\mathbf{k}_2}(\text{Fe2}) = \Gamma_1^1 + 2\Gamma_2^1 + 2\Gamma_3^1 + \Gamma_4^1 + 2\Gamma_5^1 + \Gamma_6^1 + \Gamma_7^1 + 2\Gamma_8^1 \tag{6}$$

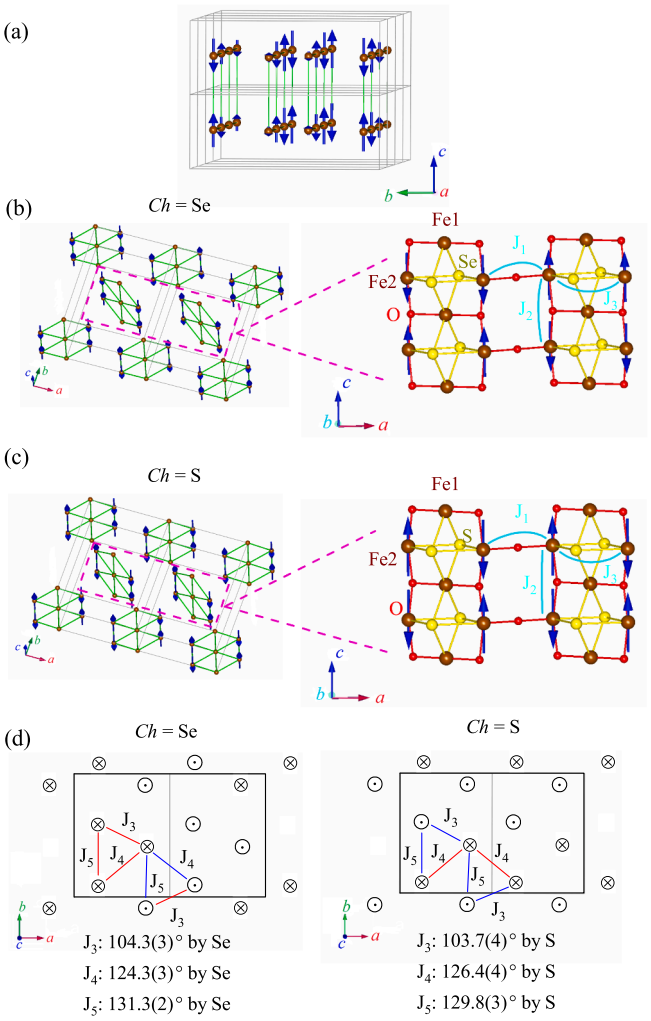

Fig. 6. (a) Magnetic structure for both samples in the $T_1 < T < T_{inc}$ regime with a propagation vector $k_{inc} = (\delta, 0, 1/2)$. (b) and (c) Magnetic structure in the $T_1 > T > T_2$ regime with a propagation vector $k_1 = (1/2, 0, 1/2)$ and (0, 0, 1/2) for the *Ch* = Se and *Ch* = S samples, respectively. For simplicity, the left panels only show the Fe ions. The right panels show the Fe-ladder structure running along the *c*-axis with bonded O and S ions. (d) A top view of the magnetic structure. ⊗ and ⊙ symbols indicate that the moments are pointing inward and outward of the drawing plane. Fe-O-Fe bond angles for the different exchange paths J_i shown in this figure - J_1: 180° for both compounds and J_2 :∼ 167.7(6)° and 166.8(4)° for the *Ch* = Se and *Ch* = S compounds, respectively. Note, that there are also Fe-*Ch*-Fe exchange paths that are associated with somewhat smaller bond angles that we omitted here.

The BVs are shown in Table 5 and 6. It can be seen that half of the Fe1 ions are paramagnetic for each IR. Since Mössbauer measurements indicate that all the Fe moments become ordered in this temperature regime [3,4], a combination of the IRs such as $\Gamma_1 + \Gamma_7$ or $\Gamma_3 + \Gamma_5$ is needed in order to realize a fully ordered state. Due to an assumed coupling of the Fe1 and Fe2 sites we restricted our refinements to the ones with the same IR for both sites. Finally, it turned out that these additional reflections can be best described by $\Gamma_3 + \Gamma_5$ for both compounds. This solution corresponds to a magnetic structure with moments constrained within the *ab*-plane. Together with the magnetic structure established below T_1 for the Fe2 ions, the final refinement shows that for the *Ch* = Se compound the Fe1 moments are lying in the *ab*-plane with M_a(Fe1) = 2.7(2) μ_B,M_b(Fe1) = 1.9(2) μ_B and M_{total}(Fe1) = 3.3(2) μ_B at 2 K. The Fe2 moments are canted from the *c*-axis with M_a(Fe2) = 1.54(9) μ_B,M_b(Fe2) = 0.3(2) μ_B,M_c(Fe2) = 3.10(4) μ_B and M_{total}(Fe2) = 3.47(6) μ_B at 2 K. The refined pattern is shown in Fig. 4(c) and the magnetic

Table 3
Nonzero IRs together with basis vectors φ_ν for the Fe2 ions at the *4h* sites in $Sr_2Fe_3Se_2O_3$ with space group *Pbam* and propagation vector $\mathbf{k}_1 = (1/2, 0, 1/2)$. The first site coordinate is (x, y, z) = (0.2577, 0.0896, 0.5000), site 2 = (-x + 1, -y + 1, z), site 3 = (-x + 1/2, y + 1/2, -z + 1), and site 4 = (x + 1/2, -y + 1/2, -z + 1).

IRs	φ_ν	component	site 1	site 2	site 3	site 4
Γ_1	φ_1	Real	(1 0 0)	(1 0 0)	(0 0 0)	(0 0 0)
	φ_2	Real	(0 1 0)	(0 1 0)	(0 0 0)	(0 0 0)
	φ_3	Real	(0 0 0)	(0 0 0)	(1 0 0)	(1 0 0)
	φ_4	Real	(0 0 0)	(0 0 0)	(0 −1 0)	(0 −1 0)
	φ_5	Real	(0 0 0)	(0 0 0)	(1 0 0)	(−1 0 0)
	φ_6	Real	(0 0 0)	(0 0 0)	(0 −1 0)	(0 1 0)
	φ_7	Real	(1 0 0)	(−1 0 0)	(0 0 0)	(0 0 0)
	φ_8	Real	(0 1 0)	(0 −1 0)	(0 0 0)	(0 0 0)
Γ_2	φ_9	Real	(0 0 1)	(0 0 −1)	(0 0 0)	(0 0 0)
	φ_{10}	Real	(0 0 0)	(0 0 0)	(0 0 1)	(0 0 −1)
	φ_{11}	Real	(0 0 0)	(0 0 0)	(0 0 1)	(0 0 1)
	φ_{12}	Real	(0 0 1)	(0 0 1)	(0 0 0)	(0 0 0)

Table 4
Nonzero IRs together with basis vectors φ_ν for the Fe2 ions at the *4h* sites in $Sr_2Fe_3S_2O_3$ with space group *Pbam* and propagation vector $\mathbf{k}_1 = (0, 0, 1/2)$. The first site coordinate is (x, y, z) = (0.2579, 0.0938, 0.5000), site 2 = (-x + 1, -y + 1, z), site 3 = (-x + 1/2, y + 1/2, -z + 1), and site 4 = (x + 1/2, -y + 1/2, -z + 1).

IRs	φ_ν	component	site 1	site 2	site 3	site 4
Γ_1	φ_1	Real	(1 0 0)	(−1 0 0)	(1 0 0)	(−1 0 0)
	φ_2	Real	(0 1 0)	(0 −1 0)	(0 −1 0)	(0 1 0)
Γ_2	φ_3	Real	(0 0 1)	(0 0 1)	(0 0 1)	(0 0 1)
Γ_3	φ_4	Real	(1 0 0)	(−1 0 0)	(-1 0 0)	(1 0 0)
	φ_5	Real	(0 1 0)	(0 −1 0)	(0 1 0)	(0 −1 0)
Γ_4	φ_6	Real	(0 0 1)	(0 0 1)	(0 0 −1)	(0 0 −1)
Γ_5	φ_7	Real	(0 0 1)	(0 0 −1)	(0 0 1)	(0 0 −1)
Γ_6	φ_8	Real	(1 0 0)	(1 0 0)	(1 0 0)	(1 0 0)
	φ_9	Real	(0 1 0)	(0 1 0)	(0 −1 0)	(0 −1 0)
Γ_7	φ_{10}	Real	(0 0 1)	(0 0 −1)	(0 0 −1)	(0 0 1)
Γ_8	φ_{11}	Real	(1 0 0)	(1 0 0)	(−1 0 0)	(−1 0 0)
	φ_{12}	Real	(0 1 0)	(0 1 0)	(0 1 0)	(0 1 0)

Table 5
Nonzero IRs together with basis vectors φ_ν for the Fe1 ions at the *2a* sites in $Sr_2Fe_3Ch_2O_3$ with space group *Pbam* and propagation vector $\mathbf{k}_2 = (0.5\ 0.5\ 0.0)$. The first site coordinate is (x, y, z) = (0 0 0).

IRs	φ_ν	component	(x, y, z)	(-x + 1/2, y + 1/2, -z)
Γ_1	φ_1	Real	(0 0 1)	(0 0 0)
Γ_3	φ_2	Real	(1 0 0)	(0 0 0)
	φ_3	Real	(0 1 0)	(0 0 0)
Γ_5	φ_4	Real	(0 0 0)	(1 0 0)
	φ_5	Real	(0 0 0)	(0 −1 0)
Γ_7	φ_6	Real	(0 0 0)	(0 0 −1)

structure is shown in Fig. 7(a). For the *Ch* = S compound, the Fe1 moments are also lying in the *ab*-plane with M_a(Fe1) = 3.39(4) μ_B,M_b(Fe1) = 1.6(2) μ_B and M_{total}(Fe1) = 3.75(9) μ_B at 2 K. The Fe2 moments are canted from the *c*-axis with M_a(Fe2) = 1.50(3) μ_B,M_b(Fe2) = 0.19(8) μ_B, M_c(Fe2) = 3.27(2) μ_B and M_{total}(Fe2) = 3.60(2) μ_B at 2 K. The refined pattern is shown in Fig. 5(c) and the magnetic structure is shown in Fig. 7(b). The Fe1 moments are pointing approximately towards the coordinated O ions (for both compounds).

The incommensurate magnetic structure suggests the existence of the frustration within the Fe2 sublattice, see Fig. 6(d). For the *Ch* = Se

Table 6
Nonzero IRs together with basis vectors φ_ν for the Fe2 ions at the *4h* sites in $Sr_2Fe_3Ch_2O_3$ with space group *Pbam* and propagation vector $\mathbf{k}_2 = (0.5, 0.5, 0.0)$. The first site coordinate is (x, y, z) = (0.2577, 0.0896, 0.5000), site 2 = (-x + 1, -y + 1, z), site 3 = (-x + 1/2, y + 1/2, -z + 1), and site 4 = (x + 1/2, -y + 1/2, -z + 1).

IRs	φ_ν	component	site 1	site 2	site 3	site 4
Γ_1	φ_1	Real	(0 0 1)	(0 0 0)	(0 0 0)	(0 0 1)
Γ_2	φ_2	Real	(1 0 0)	(0 0 0)	(0 0 0)	(−1 0 0)
	φ_3	Real	(0 1 0)	(0 0 0)	(0 0 0)	(0 −1 0)
Γ_3	φ_4	Real	(1 0 0)	(0 0 0)	(0 0 0)	(1 0 0)
	φ_5	Real	(0 1 0)	(0 0 0)	(0 0 0)	(0 1 0)
Γ_4	φ_6	Real	(0 0 1)	(0 0 0)	(0 0 0)	(0 0 −1)
Γ_5	φ_7	Real	(0 0 0)	(1 0 0)	(1 0 0)	(0 0 0)
	φ_8	Real	(0 0 0)	(0 −1 0)	(0 −1 0)	(0 0 0)
Γ_6	φ_9	Real	(0 0 0)	(0 0 −1)	(0 0 1)	(0 0 0)
Γ_7	φ_{10}	Real	(0 0 0)	(0 0 −1)	(0 0 −1)	(0 0 0)
Γ_8	φ_{11}	Real	(0 0 0)	(1 0 0)	(−1 0 0)	(0 0 0)
	φ_{12}	Real	(0 0 0)	(0 −1 0)	(0 1 0)	(0 0 0)

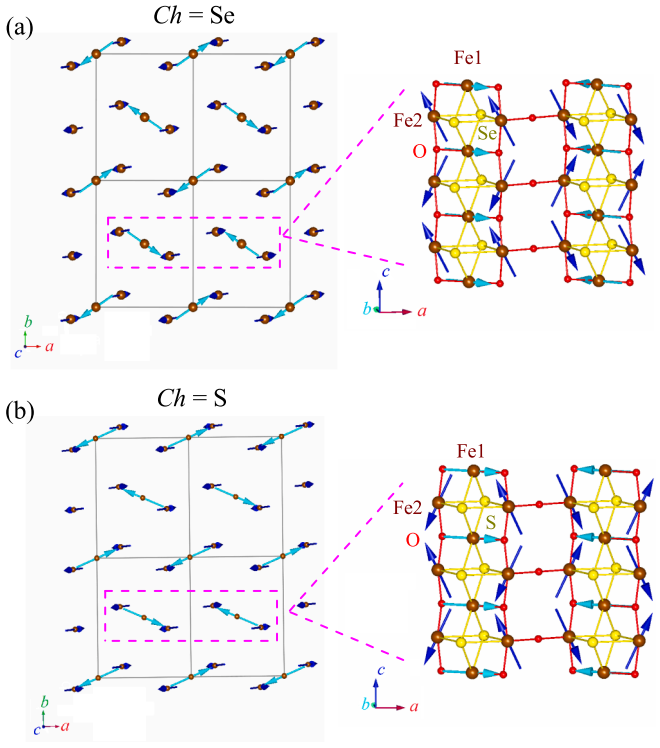

Fig. 7. Magnetic structure in the $T < T_2$ regime for (a) *Ch* = Se and (b) *Ch* = S samples. The left panels are top views, while the right panels are side views showing the Fe-ladder structure running along the *c*-axis with bonded O and *Ch* ions.

compound half of the J_4/J_5-pairs are antiferromagnetically aligned whereas the other half is ferromagnetically aligned. However, there is a different alignment for the *Ch* = S compound, see Fig. 6(d). It seems that small variations of the local structure results in distinct magnetic structures in the $T_2 < T < T_1$ regime. The magnetic ground state can also be very sensitive to external perturbations. Magnetic susceptibility measurements for both compounds show a ferri/ferromagnetic-like transition below T_{inc} (denoted as T_{N1} in Ref. [3]) with an external magnetic field of 3 T. However, our zero-field neutron diffraction measurements reveal an antiferromangetic structure with zero net moments. Thus, it can be expected that the magnetic field induces an antiferromagnetic to ferri/ferromagnetic transition in these compounds,

which is especially obvious for the Ch = Se compound from the susceptibility measurement.

The ordered magnetic moments at the Fe1 and Fe2 sites are distinct and also lower than the expected values for a Fe^{2+} ion in the high spin state. Besides covalence effects or thermal fluctuations and/or disorder also frustration could be responsible for this. The difference between the two sites could be due to the two very different local coordinations of these Fe ions.

Finally, we have no indications for a structural symmetry lowering around T_{inc} and T_1. However, the temperature dependence of the lattice parameters which is shown in Fig. 3 exhibits weak anomalies of the lattice constants for both compounds (Ch = S, Se) at the magnetic transition temperatures which shows that these compounds are in some extent prone to magnetoelastic coupling.

4. Summary

In summary, we have studied the phase diagram and the appearing magnetic structures in the $Sr_2Fe_3Ch_2O_3$ system (Ch = S) by means of powder neutron diffraction and compared it to the Ch = Se system. Interestingly, the magnetic propagation vectors exhibit a lock-in to different commensurate values in these two compounds with Ch = S and Se: wheras the incommensurability δ of the Ch = Se compound increases with decreasing temperature until it attains the half-integer value of 1/2, for Ch = S the corresponding incommensurability jumps suddenly to the integer value of zero. This results in different magnetic structures that are arising from a qualitatively different ferro- or antiferromagnetic coupling of certain Fe-chains which is obviously the consequence of (small) changes in the structure of both compounds that cause a variation of the balance of the different exchange interactions occuring in these materials.

CRediT authorship contribution statement

H. Guo: Data curation, Writing - original draft, Visualization, Investigation, Methodology, Software, Formal analysis. **M.T. Fernández-Díaz:** Investigation. **K.T. Lai:** Resources. **M. Valldor:** Resources. **A. C. Komarek:** Conceptualization, Supervision, Writing - review & editing, Visualization.

Declaration of Competing Interest

The authors declare that they have no known competing financial interests or personal relationships that could have appeared to influence the work reported in this paper.

Acknowledgement

We thank L. H. Tjeng for helpful discussions.

References

[1] E. Dagotto, T.M. Rice, Science 271 (1996) 618, https://science.sciencemag.org/content/271/5249/618.full.pdf.
[2] H. Takahashi, A. Sugimoto, Y. Nambu, T. Yamauchi, Y. Hirata, T. Kawakami, M. Avdeev, F. Matsubayashi, K.and Du, C. Kawashima, H. Soeda, S. Nakano, Y. Uwatoko, Y. Ueda, T.J. Sato, and K. Ohgushi, Nature Mater. 14, 1008 (2015).
[3] K.T. Lai, P. Adler, Y. Prots, Z. Hu, C.-Y. Kuo, T.-W. Pi, M. Valldor, Inorg. Chem. 56 (2017) 12606.
[4] S.J. Cassidy, F. Orlandi, P. Manuel, J. Hadermann, A. Scrimshire, P.A. Bingham, S. J. Clarke, Inorg. Chem. 57 (2018) 10312.
[5] A. Gubkin, E. Sherokalova, L. Keller, N. Selezneva, A. Proshkin, E. Proskurina, N. Baranov, J. Alloys Compd. 616 (2014) 148.
[6] J. Rodríguez-Carvajal, Physica B 192 (1993) 55.
[7] A.S. Wills, Physica B 276–278 (2000) 680.
[8] H. Guo, M.-T. Fernández-Díaz, A.C. Komarek, S. Huh, P. Adler, M. Valldor, Eur. J. Inorg. Chem. 2017 (2017) 3829.